Materials Letters 120 (2014) 151–154

Contents lists available at ScienceDirect

Materials Letters

journal homepage: www.elsevier.com/locate/matlet

Indentation size effect of stress exponent and hardness in homogeneous duplex eutectic 80Au/20Sn

Wensheng Liu, Yikai Wang, Yunzhu Ma*, Yufeng Huang, Ya Tang, Fan Cheng

State Key Laboratory of Powder Metallurgy, Central South University, Changsha 410083, PR China

ARTICLE INFO

Article history:
Received 28 November 2013
Accepted 11 January 2014
Available online 21 January 2014

Keywords:
Indentation and hardness
Indentation size effect
80Au/20Sn
Stress exponent
Creep

ABSTRACT

The indentation size effect (ISE) of creep stress exponent and hardness in homogeneous duplex eutectic 80Au/20Sn was studied by nanoindentation, using constant load/holding (CL) and continuous multi-cycle (CMC) loading modes, respectively. The stress exponent of each fixed load decreases first and then increases as the indentation depth increases. The stress exponent for the same strain rate range increases with the indentation depth increasing. The result of CMC indicates that Nix-Gao's overestimates the hardness of 80Au/20Sn for small indentations. A revised model incorporating enlarged effective plastic zone and the maximum geometrically necessary dislocation density was achieved to describe the relationship between hardness and indentation depth.

1. Introduction

Due to its excellent high temperature shear strength, high electrical and thermal conductivity, superior resistance to corrosion and free flux soldering, eutectic 80Au/20Sn are widely used in high-power optoelectronics and hermetic sealing applications [1–3]. However, at room temperature (T=298 K), 80Au/20Sn has high homologous temperature ($T/T_m > 0.5$), at which creep deformation becomes critical for connection reliability. On the other hand, the dimensions of electronic devices are approaching to nano-scale to obtain high packing density. It is important to gain an insight into the micro/nano-mechanical properties, such as stress exponent (n), hardness (H) and young's modulus (E), of solder alloys to design reliable devices. Recently, nanoindentation has been widely used to study micro/nano-mechanical behaviors of Sn-based solder alloys, such as Sn–Bi [4,5] and Sn–Ag–Cu [6,7]. But limited attention has been paid to the micro/nano-mechanic behaviors of AuSn solder [8]. On the other hand, extensive studies have shown that H significantly decreases with increasing indentation depth, i.e., the ISE of hardness. Yet, few reports have been published concerning the possibility of ISE of indentation creep stress exponent, which is closed related to the creep mechanism.

The ISE of hardness was commonly explained by Nix–Gao's geometrically necessary dislocation (GNDs) model [9]. However, many researchers, such as Swadener et al. [10] and Feng et al. [11], have reported overestimations of hardness for small indentation by Nix–Gao's model. They explained the overestimations as follows: due to strong repulsive force, GNDs would spread out beyond the hemisphere underneath the indenter; therefore the model overestimates the GNDs density (ρ_G), underestimates the plastic zone and the hardness. Although Feng et al. [11] and Huang et al. [12] have modified the Nix–Gao's model taking the effect of spread-out plastic zone and the overestimated ρ_G into consideration, respectively, no researchers have quantitatively analyzed those two specified factors at the same time.

In this study, we investigate the ISE of both creep stress exponent and hardness of homogeneous duplex eutectic 80Au/20Sn solder alloy and propose a new model to quantify the ISE of hardness. And the revised model fits well with experimental data.

2. Experimental

Eutectic 80Au/20Sn samples were prepared from high-purity tin (99.99%) and gold (99.99%) via a vacuum melting furnace. To obtain homogeneous structure and eliminate effect of solidified residual stress, the samples were annealed at 473 K for 5 h. Emery paper and fine alumina powder were used to polish the as-cast and annealed samples with mirror-like surfaces to meet the requirements for nanoindentation. Microstructure characterizations of both the as-cast and homogenized samples were carried out on a FEI Nova Nano230 scanning electron microscopy (SEM). The phases presented in the solder were characterized using Energy Dispersive Spectroscopy (EDS) and X-ray diffractometer (XRD). Nanoindentations were conducted on an Ultra Nanoindentation tester using Berkovich indenter (tip radius $R \approx 100$ nm) calibrated by fused silica. Room temperature indentation creep tests were performed at the same loading rate 4 mN/s with peak

* Corresponding author. Tel.: +86 731 888 77825.
E-mail address: zhuzipm@csu.edu.cn (Y. Ma).

0167-577X/$ - see front matter © 2014 Elsevier B.V. All rights reserved.
http://dx.doi.org/10.1016/j.matlet.2014.01.066

loads ranging from 150 mN to 400 mN. After the peak load was reached, the indenter was held for 400 s to determine creep response, during which the indentation depth–dwell time (D–T) curves could be formulated as [13]

$$h = y_0 + A_1 e^{-x/t_1} + A_2 e^{-x/t_2} + A_3 e^{-x/t_3} \quad (1)$$

Based on the nanoindentation data, the effective indentation strain rate and stress could be calculated from [14]

$$\dot{\varepsilon}_{in} = \frac{1}{h_i} \times \frac{dh_i}{dt} \quad (2)$$

$$\sigma_{in} = \frac{P}{A_c} \quad (3)$$

where h_i is the instantaneous indentation depth and A_c is the contact area, given by [15]

$$A_c = 24.56(h_i + 0.06R)^2 \quad (4)$$

The creep stress exponent (n) equals to the slope of the double logarithm plot of $\dot{\varepsilon}_{in}$versus σ_{in} under isothermal condition. Every value of n for each peak load was averaged by at least three independent indentations.

CMC test was carried out with 55 different peak loads ranging from 50 mN to 600 mN with the same loading and unloading time of 20 s. The hardness and young′s modulus was determined using the Oliver and Pharr′s method [16].

3. Results and discussion

Fig. 1(a) shows the back-scattered electron (BSE) image of as-cast eutectic 80Au/20Sn. It is evident that the microstructure of as-cast 80Au/20Sn was composed of two different lamellar-like phases. XRD pattern combined with the atom proportion revealed by EDX indicates that 80Au/20Sn solder was composed of δ-phase (AuSn, the dark constituent) and ζ′-phase (Au5Sn, the bright constituent). The distribution of ζ′-phase and δ-phase was fairly uniform after annealing. However, no AuSn2 and AuSn4 have been detected in the present study, which may well be attributed to fast mutual diffusion in Au–Sn system [17,18].

Fig. 2(a) shows D–T curves under each peak load during nanoindentation creep. The change of indentation depth at the peak load is defined as the creep displacement, which is seen to rapidly increase at the initial stage and then slow down during the remaining of the holding period. A typical fitting result by Eq. (1) is shown in Fig. 2(b). The strain rate reduces to almost a constant value after holding for 100 s, indicating that steady-state creep has been reached. The relationship of $\ln \dot{\varepsilon}_{in}$ vs. $\ln \sigma_{in}$ under the peak load 200 mN during steady-state creep is an anti-S type curve and could be divided into three stable stages, corresponding to different strain rate ranges, as shown in Fig. 2(c). There is an apparent ISE on the stress exponents. With the indentation depth increasing, stress exponent ($n = \ln \dot{\varepsilon}_{in} / \ln \sigma_{in}$) decreases from 26.93 to 19.92 and then increases to 41.06 during indentation creep under the peak load 200 mN. Similar trend was obtained under other peak loads, as shown in Fig. 2(d) and Table 1. The stress exponent higher than 10 implies that dislocation motion (including dislocation glide and climb) is the dominant creep mechanism [19]. Dislocation passes individual phase and grain boundary to generate creep deformation. At the initial steady-state creep, σ_{in} is relative high, dislocation passes through the matrix and grain boundary via gliding in the high stress regime (HSR) [20]. As the indentation depth increases, σ_{in} decreases and creep deformation gradually enters into the low stress regime (LSR) [20], during which dislocation is unable to overcome the impediment of grain boundary due to its high strength at room temperature. Therefore, those dislocations will be pinned or arrested at the grain boundary [21]. Then dislocation motion shifts into climbing to pass through the boundary to continue creep deformation and the stress exponent becomes lower than that of HSR.

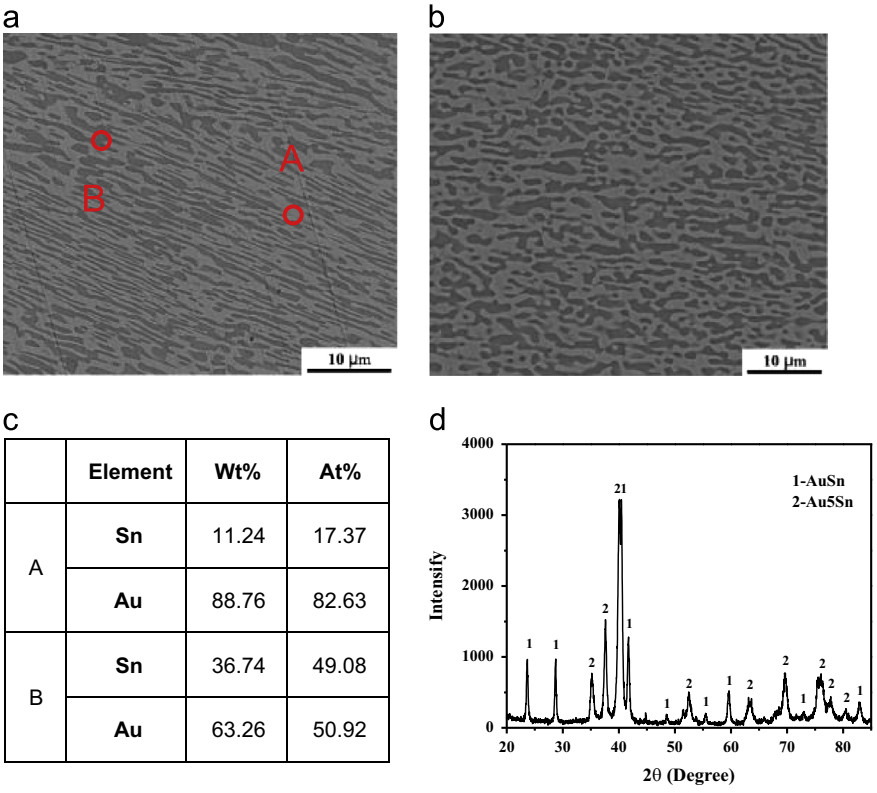

	Element	Wt%	At%
A	Sn	11.24	17.37
	Au	88.76	82.63
B	Sn	36.74	49.08
	Au	63.26	50.92

Fig. 1. BSEM of eutectic 80Au/20Sn: (a) as-cast; (b) annealed; (c) EDX analysis and (d) XRD pattern of as-cast 80Au/20Sn.

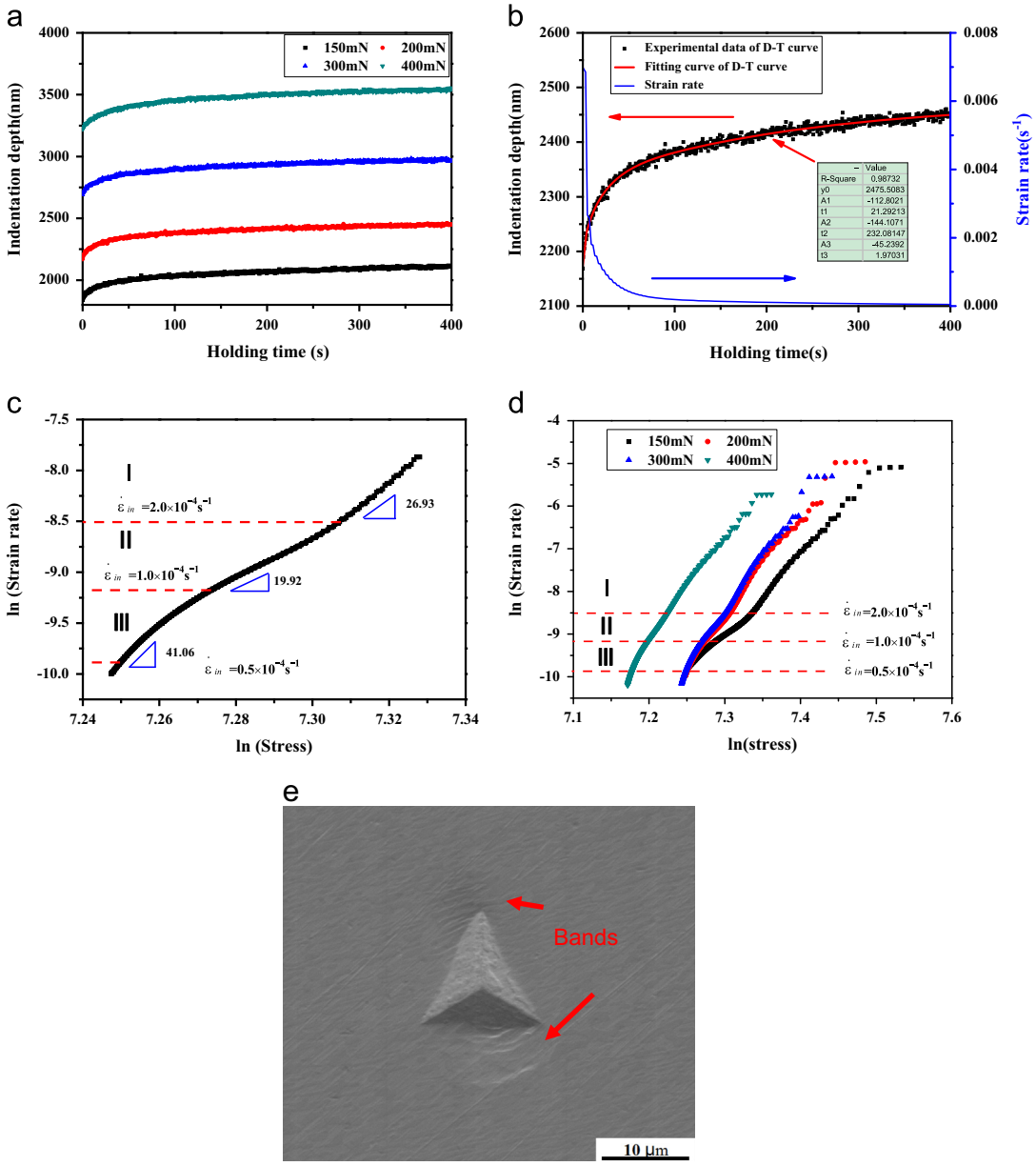

Fig. 2. (a) *D–T* curves under different peak loads; (b) fitting result and the strain rate under peak load 200 mN; and strain rate versus stress curves for: (c) 200 mN; (d) a comparison of different peak loads; (e) SEM of indentation imprint under 200 mN.

Table 1
Stress exponents and the corresponding indentation depth under different peak loads.

Peak load (mN)	2.0×10^{-4} (s^{-1})		1.0×10^{-4} (s^{-1})		0.5×10^{-4} (s^{-1})	
	h (nm)	n	h (nm)	n	h (nm)	n
150	2040.09	19.76	2092.66	13.30	> 2118.71	19.05
200	2378.13	26.93	2419.30	19.92	2447.11	41.06
300	2888.09	27.28	2935.23	22.80	2965.24	45.41
400	3451.41	28.65	3498.90	24.72	3534.80	48.69

As the indentation depth continues to increase, more dislocations are nucleated but the annihilation rate is low due to the low atom thermal motion rate at room temperature. As a result, the residual dislocations interact with each other or accumulate at the grain boundary, resulting in significant hardening effect. Thus, 80Au/20Sn alloy gains more resistance to creep and the value of stress exponent becomes higher although σ_{in} continues to decrease. It is also observed from Table 1 that the stress exponent for the same strain rate range increases with the indentation depth. This apparent size effect on stress exponent may also be ascribed to the hardening effect, whose level is proportional to the indentation depth.

Fig. 2(e) presents the SEM of typical indentation morphology of 80Au/20Sn after indentation creep tests. There are obvious wave-like pile-up bands around the regular triangle indentation imprints. It is believed that the indentation deformation is accomplished by the bulk deformation inside both AuSn and Au5Sn, during which the harder individual phases push the peripheral soft phases out and upward forming the wave-like bands.

Fig. 3 shows the result of CMC test. It can be seen that E decreases with the indentation depth until a constant value of 71.2 Gpa is reached at 3500 nm. While H decreases with the indentation depth continuously, indicating obvious ISE. Fig. 3 (c) shows the plot of H^2 versus $1/h$, suggesting a linear relation for h larger than 1500 nm, as predicated by Nix–Gao's model.

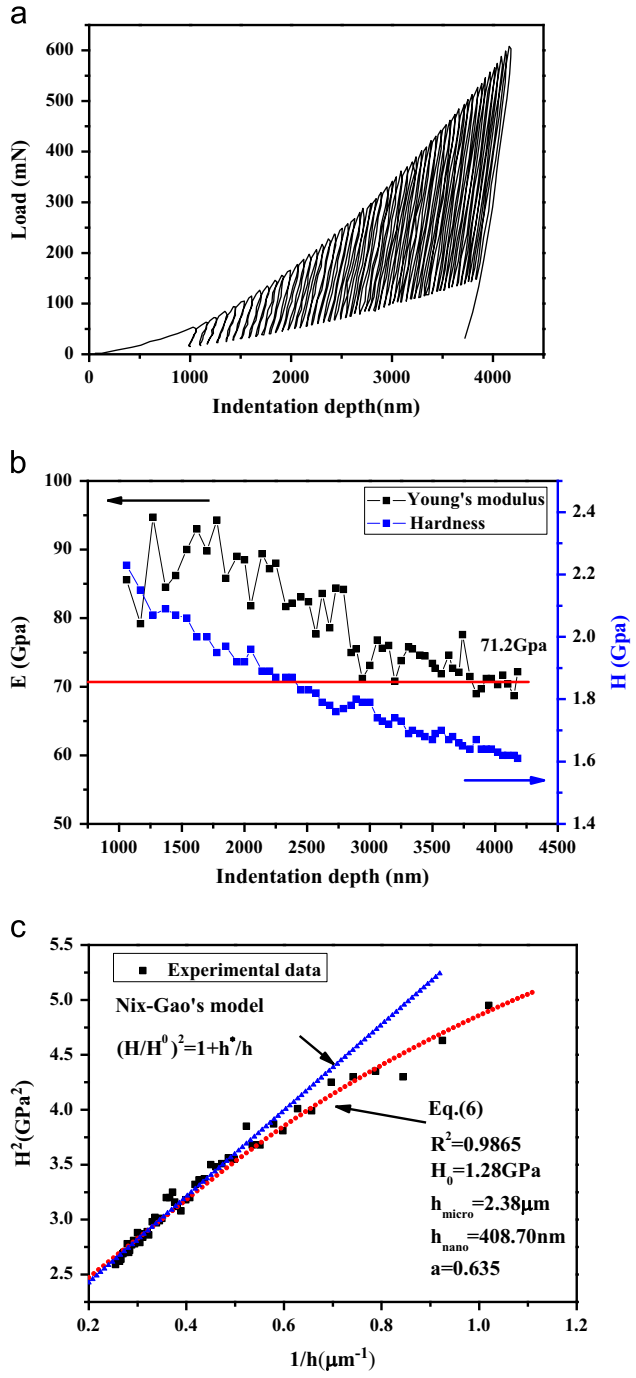

Fig. 3. (a) Load–depth curve of CMC; (b) variation of E and H with indentation depth; (c) H^2–$1/h$ curve.

However, the model overestimates H for smaller h. The factors for the overestimation lie in the basic assumptions of the model: (1) the indenter is a perfect "sharp", pyramid indenter; (2) all the GNDs are stored in a hemisphere with a radius equals to the contact radius. Besides, the model does not take into account of grain boundary effects, which is of great importance for polycrystalline materials since many grain boundaries are involved in the dislocation motion. In the present study, we have modified the contact area by Eq. (4) to exclude the influence of indenter tip radius. Thus, the overestimation may well be explained by the overestimated ρ_G and the enlarged plastic zone. Therefore, it is reasonable to introduce a maximum allowable $\rho_G^{\max}$ and effective storage radius, δr, rather than the contact radius, r, for GNDs. We simplify Feng's analysis [11] and take $\delta = 1 + e^{-a/h}$, where a is a fitting parameter. Based on Huang's model [12], we have

$$\rho_G = \rho_G^{\max} \begin{cases} 1 & h < h_{nano} \\ \frac{1}{\delta^3}\left(\frac{3h_{nano}}{2h} - \frac{h_{nano}^3}{2h^3}\right) & h \geq h_{nano} \end{cases} \quad (5)$$

where $h_{nano} = (\tan^2\theta / b\rho_G^{\max})$ is the characteristic depth for nanoindentation and is much smaller than the micron characteristic depth h_{micro}. In the present study, the dimension of indentation depth is on the order of microns. For $h > h_{nano}$, based on the Nix–Gao's method, we obtain

$$\left(\frac{H}{H_0}\right)^2 = 1 + \frac{1}{\delta^3}\left(\frac{h_{micro}}{h} - \frac{h_{nano}^2 h_{micro}}{3h^3}\right) \quad h > h_{nano} \quad (6)$$

Fig. 3(c) shows that Eq. (6) fits well with the experimental data. H_0, h_{micro} and h_{nano} of homogeneous duplex 80Au/20Sn are determined to be 1.28 Gpa, 2.38 μm and 408.70 nm, respectively. However, in the present study, the nanoindentation characteristic depth h_{nano} may have little significance since the dimensions of both phases in 80Au/20Sn are quiet large.

4. Conclusion

Both the stress exponent and the hardness of homogeneous duplex 80Au/20Sn exhibit an apparent ISE. As the indentation depth increases, the stress exponent decreases due to the decrease of indentation stress inducing dislocation glide shifts to climb and then increases because of hardening effect. The overestimation of hardness for small indentation by Nix–Gao's model could well be attributed to the enlarged plastic zone and the maximum GNDs density. The relationship of hardness and indentation depth agrees reasonable well with the revised model. The depth independent hardness and the micron-indentaiton characteristic depth of homogeneous duplex 80Au/20Sn were calculated to be 1.28 Gpa and 2.38 μm, respectively.

References

[1] Kim D, Lee CC. Mater Sci Eng A 2006;416:74–9.
[2] Liu X, Hu MH, Nguyen HK, Caneau CG, Rasmussen MH, Davis Jr RW, et al. IEEE Trans Adv Packag 2004;27:640–6.
[3] Wang C-P, Chen T-T, Fu H-K, Chang T-L, Chou P-T, Chu M-T. Microelectron Reliab 2012;52:698–703.
[4] Shen L, Septiwerdani P, Chen Z. Mater Sci Eng A 2012;558:253–8.
[5] Shen L, YU Z, CHE Z. Mater Sci Eng A 2013;561:232–8.
[6] Roshanghias A, Kokabi A, Miyashita Y, Mutoh Y, Ihara I, Fatt RG, et al. J Electron Mater 2012;41:2057–64.
[7] Han Y, Jing H, Nai S, Xu L, Tan C, Wei J. J Electron Mater 2010;39:223–9.
[8] Liu Y, Teo J, Tung S, Lam K. J Alloy Compd 2008;448:340–3.
[9] Nix WD, Gao H. J Mech Phys Solids 1998;46:411–25.
[10] Swadener J, George E, Pharr G. J Mech Phys Solids 2002;50:681–94.
[11] Feng G, Nix WD. Scr Mater 2004;51:599–603.
[12] Huang Y, Zhang F, Hwang K, Nix W, Pharr G, Feng G. J Mech Phys Solids 2006;54:1668–86.
[13] Yang S, Zhang Y-W, Zeng K. J Appl Phys 2004;95:3655–66.
[14] Goodall R, Clyne T. Acta Mater 2006;54:5489–99.
[15] Yu N, Polycarpou AA, Conry TF. Thin Solid Films 2004;450:295–303.
[16] Oliver WC, Pharr GM. J Mater Res 1992;7:1564–83.
[17] Wei X, Wang R, Feng Y, Zhu X, Peng C. Rare Metals 2011;30:627–32.
[18] Yoon J-W, Jung S-B. Microelectron Eng 2007;84:2634–9.
[19] Langdon TG. Metall Mater Trans A 2002;33:249–59.
[20] Han Y, Jing H, Nai S, Tan C, Wei J, Xu L, et al. J Phys D Appl Phys 2009;42:125411.
[21] Huang P, Wang F, Xu M, Xu K, Lu T. Acta Mater 2010;58:5196–205.